MODAL-BASED IDENTIFICATION OF ACOUSTIC EMISSION SOURCES IN THE PRESENCE OF ELECTRONIC NOISE [#∞]

M. A. HAMSTAD[1,2] and A. O'GALLAGHER[1]

[1] National Institute of Standards and Technology, Materials Reliability Division (853), 325 Broadway, Boulder, CO 80305-3328 USA; [2] Department of Engineering, University of Denver, Denver, CO 80208 USA.

Abstract

Based on the results of an earlier study, a specific scheme was demonstrated to identify acoustic emission (AE) source types using ratios of Lamb-wave modal amplitudes from two radiation directions in an aluminum plate 4.7 mm thick. The modal amplitudes were obtained from certain peak magnitudes of wavelet transforms (WT) of the AE signals at a propagation distance of 180 mm. The peak magnitudes were taken from energetic frequency-mode combinations. These combinations were the fundamental modes A_0 at 60 kHz, S_0 at 270 kHz and S_0 at 522 kHz. The AE signal database was obtained using a validated finite element model (FEM) for three different source types, each located at six or seven depths in the plate, which had large lateral dimensions. The technique of source identification was demonstrated using ratios of the WT-determined modal magnitudes of the signals at a radiation angle of 45˚ divided by those from a 0˚ angle. Then, the effect on source identification of adding electronic noise (sensor/preamplifier) to the FEM signals was studied. Due to the random nature of the experimental wideband noise, a statistical study was necessary. At each signal-to-noise (S/N) ratio, 50 cases were examined for certain depths of each source type. The percentage of correct source identifications was determined as a function of the S/N ratio. To obtain a high percentage of correct identifications, a S/N ratio of at least six to one was found to be necessary.

Keywords: acoustic emission; acoustic emission modeling; AE; electronic noise; finite-element modeling; modal AE; source identification; wavelet transform; wideband acoustic emission.

1. Introduction

In a previous publication [1], a technique to identify acoustic emission (AE) sources in a plate sample was demonstrated. The technique was based on the use of ratios of peak magnitudes at certain energetic frequency-mode combinations obtained from wavelet transforms (WT) of the AE signals. The WT-based peak magnitudes correspond to the magnitude of specific Lamb modes at energetic frequencies. The ratios were formed from the wavelet transforms of the AE signals present at various radiation angles from the AE source. The approach was developed and validated using far-field (fully developed Lamb modes) AE signals, which were generated by finite-element modeling (FEM) in a plate of large lateral dimensions. Since the forward-modeling FEM technique starts with fully defined AE sources, the signal processing results could be related to different source types in an unambiguous fashion. This signal-processing approach presumes a known source location relative to the location of the pseudo-AE sensors. Currently the technique has been demonstrated for a uniform propagation distance to each sensor. In

the future we plan to extend the technique to cases where the propagation distance to the sensors varies.

The purpose of the study presented here was to examine the impact of electronic noise on the accuracy of the source-identification approach. The authors were unable to locate any previous references of such studies. Since in real AE applications the signals that are measured result from the superposition of the source-based displacement waves and the electronic noise of the sensor-preamplifier combination, the usefulness of the approach will depend on its sensitivity to the signal-to-noise (S/N) ratio. In the previous publication [1], the numerical noise in the FEM-generated AE signals had no real effect since it was about three orders of magnitude below the signal amplitudes.

2. The FEM-based AE Signal Database and Signal Processing

The previous publication [1] along with its references should be consulted for details on the database and signal processing. Briefly, the FEM signals (out-of-plane displacements of the top surface of the plate) from buried dipole sources were generated in an aluminum plate (1 m x 1 m x 4.7 mm). The AE signals in the database were obtained at a propagation distance of 180 mm for seven in-plane radiation angles (0°, 12°, 22.5°, 45°, 67.5°, 78°, and 90°). Three AE source types composed the database subset: (a) a single in-plane dipole in 0° direction (x-axis, the presumed applied stress direction); (b) a microcrack initiation with major axis in 0° direction; and, (c) a shear about the in-plane y-axis with the shear directions at 45° to the x-axis with no net moment. The depths (from the top of the plate surface) to the modeled sources were 2.35, 2.037, 1.723, 1.41, 1.097, and 0.783 mm for all three source types. Additionally, the in-plane dipole had one more source depth of 0.47 mm.

All of the FEM-calculated AE signals were processed in the following fashion. Prior to performing the wavelet transform, all the FEM-calculated signals were numerically filtered with a 40 kHz four-pole Butterworth high-pass filter. Each filtered FEM signal had a WT performed [with the parameters listed in Ref. 1] upon it using an AGU-Vallen software program [see Ref. 2]. The resulting output for each WT consisted of numerical values for the WT magnitude as a function of both time (source operation time zero to 150 μs with 0.1 μs increments) and frequency (0 to 700 kHz in 3 kHz wide increments). This output can be viewed numerically in a spreadsheet format or in a more qualitative, graphic format where various colors are used to indicate the WT magnitude on a frequency-vs.-time plot. For each WT, several features were extracted and recorded for energetic regions (largest WT magnitudes) of the WT results. First the overall absolute peak WT magnitude was recorded. Then, the predominant mode (A_0 or S_0) was determined and recorded at the previously documented [1, 3] three key frequencies of 60, 270 and 522 kHz by use of superimposed group-velocity curves. Additionally, the peak WT magnitude (modal magnitude) at each frequency was recorded. These features, as extracted at these three key energetic frequencies, provided the raw data for the source identification scheme.

3. Terminology and Related Discussion

The frequency having the greatest peak WT magnitude as a function of time was defined as the “primary” frequency for each WT; in a similar manner, the other two frequencies examined were ranked with respect to their peak WT magnitudes (in descending order) as “secondary” and “tertiary.” It was observed that when the primary frequency occurred at 60 kHz, the mode that corresponded to the arrival time of the peak WT magnitude was always A_0, whereas when the

primary frequency occurred at 270 kHz or 522 kHz, its mode was always S_0. These observations did not hold for the modes that were associated with the secondary- and tertiary-frequency WT peaks, but the modes were always either A_0 or S_0.

4. Summary of Single-Mode WT Ratio Approach for Source Identification

In the previous publication [1], the radiation pattern of the peak WT magnitudes (as normalized by the zero-degree direction value) for a fixed frequency and mode was found to be almost totally independent of the depth of the source. Also for particular key frequencies and modes, it was determined that the radiation pattern changes as a function of the AE source type. Thus, among the three source types studied (in-plane dipole, microcrack initiation, and 45° shear without a moment) and for the six or seven depths considered, it was observed that the source type could be uniquely identified by certain simple ratios of peak WT magnitudes at two selected radiation angles by use of the primary frequency-mode combination, and in some cases additionally by use of the secondary frequency-mode information. Figures 1 through 4 (shown with new figure numbers here), from the previous work [1], show the WT peak magnitude ratios for each combination of a given frequency, source type and mode as a function of the two radiation directions for each ratio. In subsequent discussion in this paper, the term "angle ratios" is used as shorthand to refer to the ratios of the WT peak magnitudes in two radiation directions.

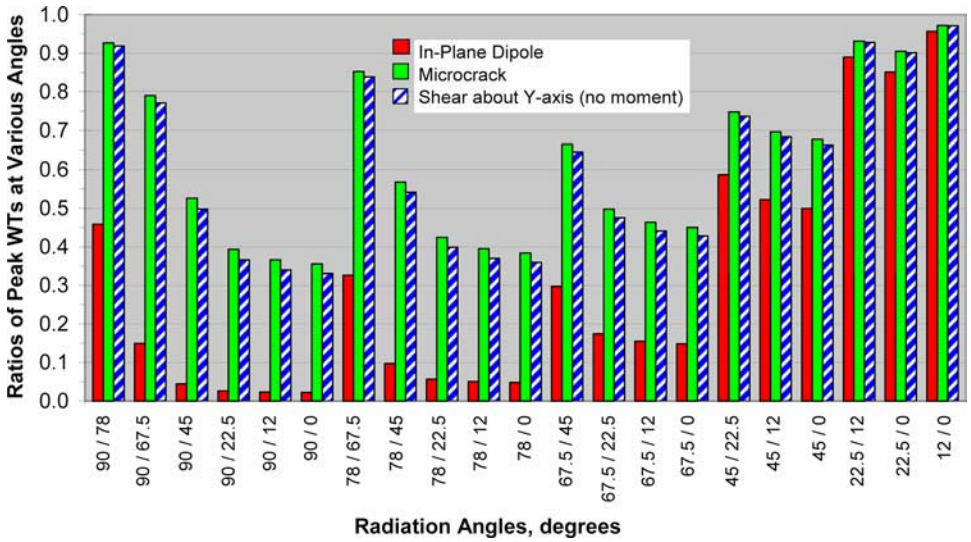

Fig. 1 Angle ratios of peak WT magnitudes for A_0 mode at 60 kHz at various radiation angles for all three source types for 180 mm propagation distance

5. Electronic Noise Effects on Source Identification by Single-Mode WT Magnitude Ratios for Various Radiation Angles

The successful application [1] of WT results to distinguish different AE source types depends on WT peak magnitudes (modal magnitudes) at the three key frequencies of 60, 270 and 522 kHz in a 4.7 mm thick aluminum plate. Thus, the primary focus in this section is WT peak magnitudes rather than AE signal magnitudes. Since the distinctions [1] between the source types depend on different "angle ratios" within a single mode at a time, the focus was on single-mode WT peak values as a function of the factors of source type, source depth and radiation angle. Figures 5, 6 and 7 show the pertinent WT-determined modal magnitudes versus the source depth for each of the three source types at a 0˚-radiation angle and a 180 mm propagation distance. For example, when the sources are located near the mid-plane these figures quantitatively show when

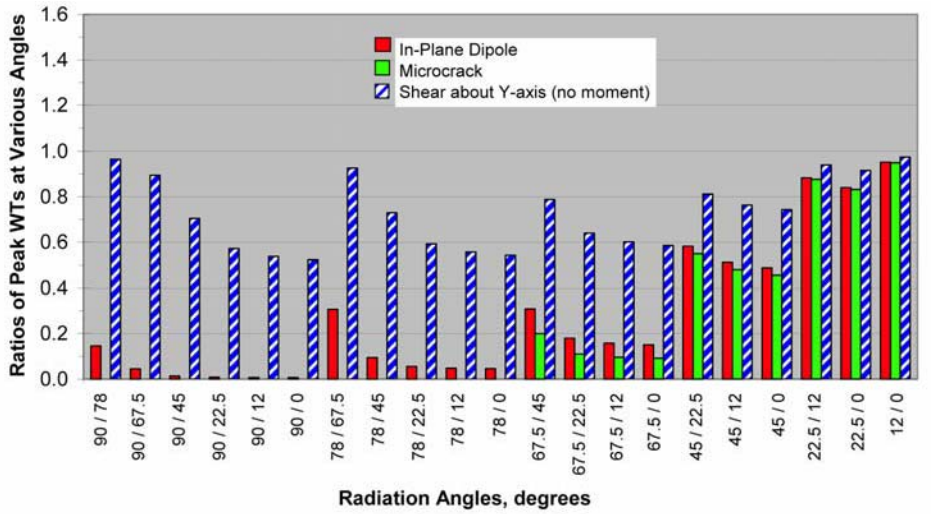

Fig. 2 Angle ratios of peak WT magnitudes for S_0 mode at 522 kHz at various radiation angles for all three source types for 180 mm propagation distance.

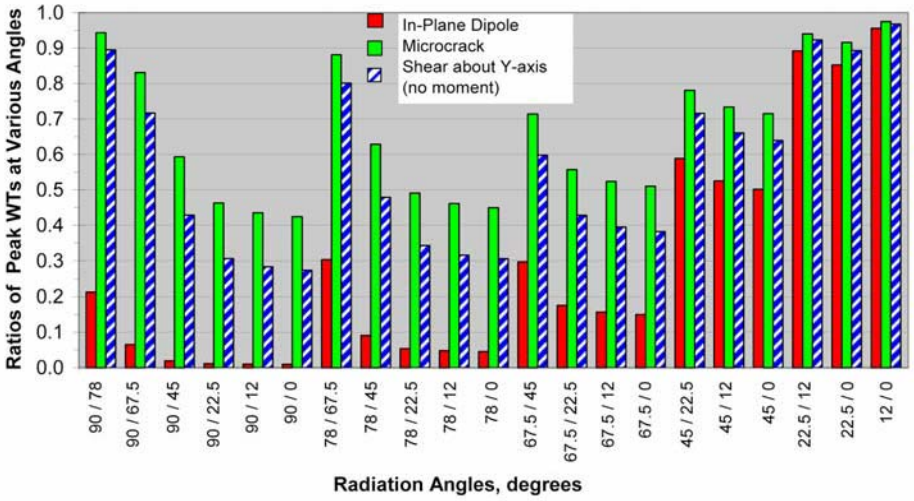

Fig. 3 Angle ratios of peak WT magnitudes for A_0 mode at 270 kHz at various radiation angles for all three source types for 180 mm propagation distance.

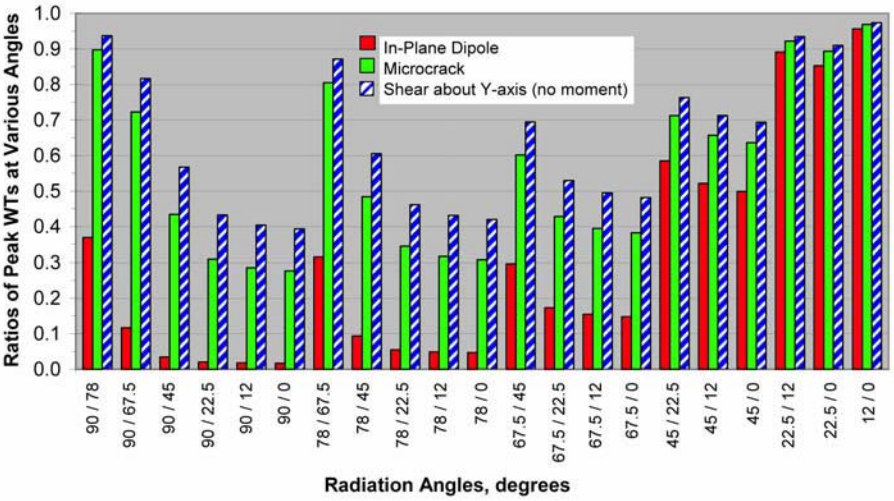

Fig. 4 Angle ratios of peak WT magnitudes for S_0 mode at 270 kHz at various radiation angles for all three source types for 180 mm propagation distance.

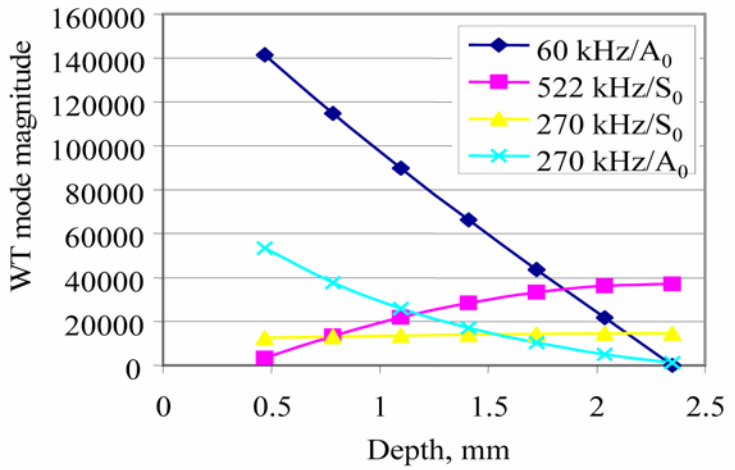

Fig. 5 Modal magnitudes for 0ºdirection, in-plane dipole, 180 mm distance.

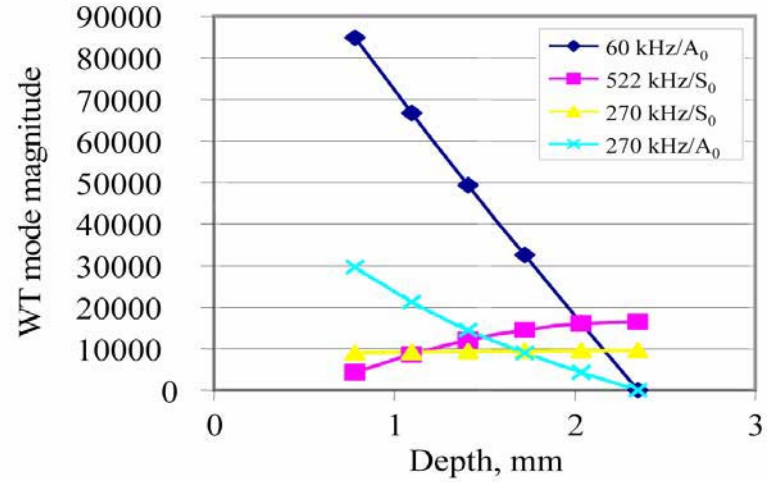

Fig. 6 Modal magnitudes for 0ºdirection, microcrack, 180 mm distance.

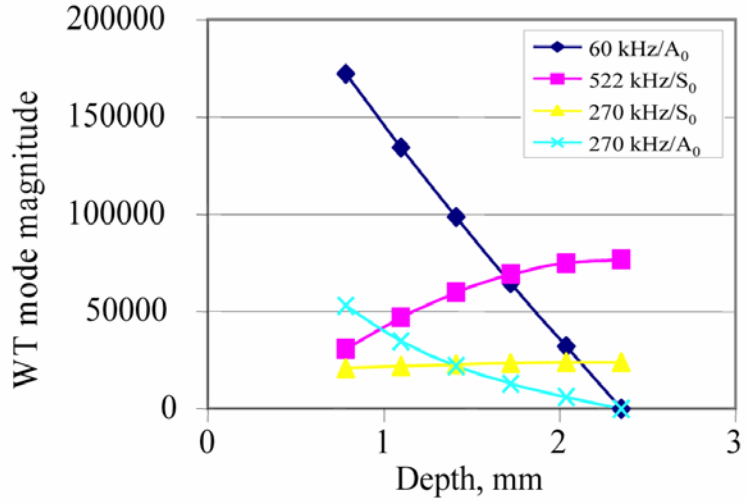

Fig. 7 Modal magnitudes for 0ºdirection, shear, 180 mm distance.

the WT magnitudes for A_0 at 60 kHz and A_0 at 270 kHz become small or not identifiable. Thus, if electronic noise were present, for sources near the mid-plane, the source distinctions shown in Figs. 1 and 3 might not be present due to the potential for noise to significantly alter the magni-

tudes of the WT peaks. On the other hand, Figs. 5, 6 and 7 quantitatively show that, for sources located nearer the surface, the WT peak magnitudes for S_0 at 522 kHz and S_0 at 270 kHz become small or not identifiable. Thus for similar reasons, the source distinctions shown in Figs. 2 and 4 may not be useable when electronic noise is present for near surface sources.

Figures 5 through 7 show that, for the three source types, the primary frequency is either 60 or 522 kHz. In certain cases two frequency-mode combinations were required to uniquely identify a source type [1]. Thus, from the point of view of maximizing S/N ratios, it is clear from Figs. 5, 6 and 7 that when a second combination is required, the 270 kHz modes should be used as the lower-amplitude second mode. For example, with an in-plane dipole (IPD) source at a depth of 0.783 mm, A_0 at 270 kHz might be expected to provide a better S/N ratio than S_0 at 522 kHz.

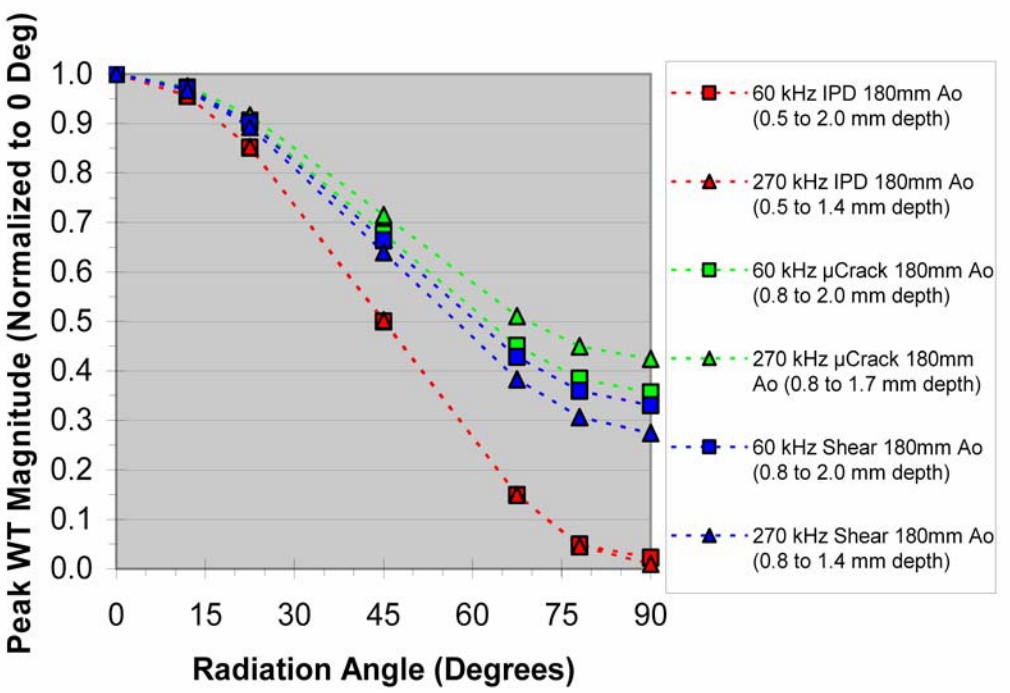

Fig. 8 Normalized peak WT magnitudes for A_0 mode (averaged for multiple depths) for all three source types for 180 mm propagation distance.

To examine the final factor affecting the WT magnitude as related to S/N ratio concerns, the four frequency/mode combinations (in Figs. 1 through 4) were examined as a function of radiation angle. Figure 8 shows the normalized WT peak magnitudes (averaged for the multiple depths shown in the figure) versus the radiation angle at the 180 mm propagation distance for the relevant frequencies (60 and 270 kHz) of the A_0 mode. Also, Fig. 9 shows the normalized and averaged WT peak magnitudes at 180 mm for the relevant frequencies (270 and 522 kHz) of the S_0 mode. The WT peak magnitudes were normalized by the zero-degree magnitudes. In general, these two figures show that the largest-magnitude decrease with increasing radiation angles takes place for the in-plane dipole source. The total decrease for this source type is about 98 % for all of the frequency/mode combinations. In addition S_0 at 522 kHz for the microcrack initiation source also experiences a large decrease. For all three source types, most of the magnitude decrease occurs from 22.5 to 67.5 degrees at all four frequency/mode combinations.

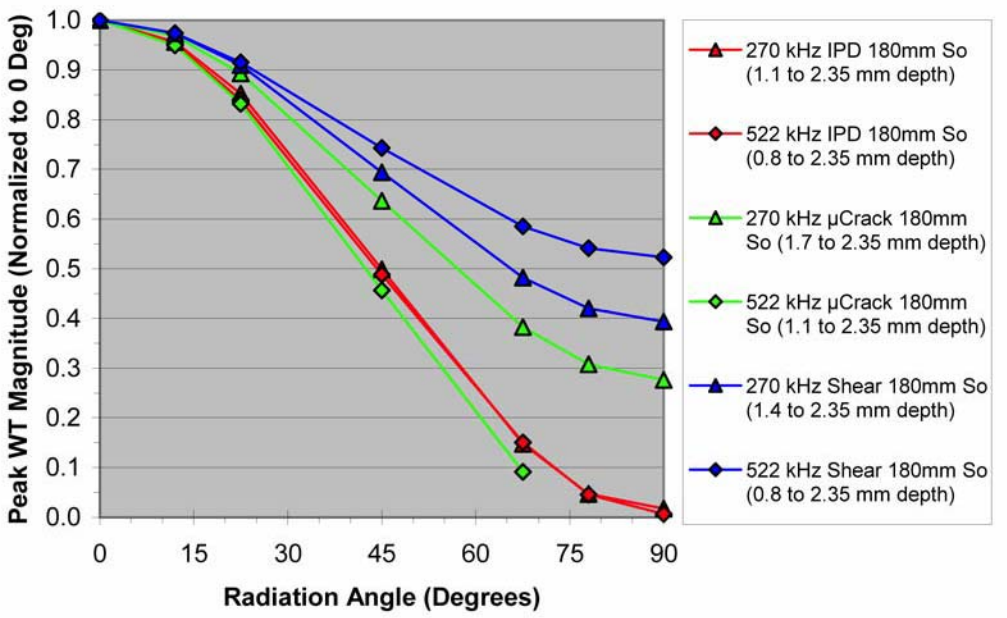

Fig. 9 Normalized peak WT magnitudes for S_0 mode (averaged for multiple depths) for all three source types for 180 mm propagation distance.

6. Discussion of Radiation Angle Choices to form the Source Identification Ratios

The WT modal peak magnitude losses (Figs. 8 and 9) with increasing (0˚ to 90˚) radiation angle are possibly the most important aspect to consider when electronic noise is present. But, it is not just the loss with increasing angle that is a potential problem. The ability to distinguish the source types by the "angle ratios" as illustrated in Figs. 1 through 4 is critical. Since the presence of noise will have the least effect on the zero-degree direction peak WT magnitudes (which were always the largest), one of the angles selected for the WT magnitude ratio should be the zero-degree direction. With this choice, it is likely that only the second angle required to form the ratio will be most strongly affected by electronic noise. This approach is more desirable than having both WT peak magnitudes that are used to calculate the ratio being strongly affected. Thus, the key choice is the second angle, which is greater than zero degrees.

Straightforward analysis demonstrated that with the current radiation angles the best choice for the second angle would be either 45˚ or 67.5˚. If 45˚ or 67.5˚ is chosen as the second angle, then there are some significant ratio distinctions between source types that are potentially resistant to small noise-induced "angle ratio" errors. For example, using the 45˚/0˚ "angle ratio" from A_0 at 60 kHz, a difference of (Fig. 1) about 32% (percent based on the no-noise ratio and the closest alternate source type) is present between the in-plane dipole and either the microcrack or shear sources. At this same "angle ratio", the S_0 at 522 kHz ratio exhibits (Fig. 2) a difference of about 34% between the shear source and either an in-plane dipole or a microcrack initiation source. For the alternate "angle ratio" at 67.5˚/0˚, the equivalent results are about 190% for the in-plane source as compared to the other two possible source-type choices for A_0 at 60 kHz, and about 74% between a shear source and either the in-plane dipole or the microcrack source for S_0 at 522 kHz. These results suggest that a choice of 67.5˚ as the second angle would tolerate greater noise-induced ratio errors without resulting in incorrect source-type determinations.

Table 1 For mode and frequency combinations: (a) 45/0 degree average "angle ratios" and [ranges]; (b) 67.5/0 degree average "angle ratios" and [ranges]; (c) source depths (mm) averaged to obtain the values in part (a); (d) source depths (mm) averaged to obtain the values in part (b).

(a)

Source type	A_0/60 kHz	A_0/270 kHz	S_0/270 kHz	S_0/522 kHz
In-plane dipole	0.50 [0.50-0.50]	0.50 [0.50-0.50]	0.50 [0.50-0.50]	0.49 [0.48-0.49]
45 Deg. Shear	0.66 [0.66-0.67]	0.64 [0.62-0.65]	0.69 [0.69-0.70]	0.74 [0.74-0.75]
Microcrack	0.68 [0.67-0.68]	0.71 [0.70-0.73]	0.64 [0.64-0.64]	0.46 [0.44-0.47]

(b)

Source type	A_0/60 kHz	A_0/270 kHz	S_0/270 kHz	S_0/522 kHz
In-plane dipole	0.15 [0.15-0.15]	0.15 [0.15-0.15]	0.15 [0.15-0.15]	0.15 [0.15-0.15]
45 Deg. Shear	0.43 [0.43-0.43]	0.38 [0.37-0.40]	0.48 [0.48-0.48]	0.59 [0.58-0.60]
Microcrack	0.45 [0.45-0.45]	0.51 [0.48-0.54]	0.38 [0.38-0.39]	0.09 [0.08-0.10]

(c)

Source type	A_0/60 kHz	A_0/270 kHz	S_0/270 kHz	S_0/522 kHz
In-plane dipole	2.037-0.47	1.41-0.47	2.35-1.097	2.35-0.783
45 Deg. Shear	2.037-0.783	1.41-0.783	2.35-1.41	2.35-0.783
Microcrack	2.037-0.783	1.723-0.783	2.35-1.723	2.35-1.41

(d)

Source type	A_0/60 kHz	A_0/270 kHz	S_0/270 kHz	S_0/522 kHz
In-plane dipole	2.037-0.47	1.41-0.47	2.35-1.097	2.35-0.783
45 Deg. Shear	2.037-0.783	1.41-0.783	2.35-1.41	2.35-1.097
Microcrack	2.037-0.783	1.723-0.783	2.35-1.723	2.35-1.723

7. Development of a Quantitative Source Identification Scheme for Noise-free Signals

To continue this evaluation of the effect of electronic noise a quantitative "scheme" to analyze and identify all the noise-free signals in the three-source-type database was developed. This "scheme" was then used for two purposes. The first purpose was to determine which "angle ratio" (45˚/0˚ or 67.5˚/0˚) best identified the noise-free signal sources. Then, the noise-free ratio values for the best "angle ratio" were used (in a later section) to determine when significant identification errors occurred when the signal plus noise data were analyzed with the same "scheme." To assist in the development of this "scheme", Table 1 was created. This table for the noise-free signals gives the average "angle ratio" values as well as their ranges for the 45˚/0˚ (a) and 67.5˚/0˚ (b) angles. In addition the table provides [(c) and (d)] the applicable depths over which the "angle ratios" were averaged. After development, the "scheme" was used to analyze each pair (from the two radiation angles) of AE signals as if their source type was *unknown*. Briefly, the "scheme" was to first find the primary frequency/mode for the zero-degree radiation direction. Then the WT peak magnitude in this direction was divided into the WT peak magnitude of the same frequency/mode combination from the second selected radiation direction (either 45˚ or 67.5˚) to form a so-called "primary" "angle ratio". This calculated ratio was then compared with the values in table 1 (which more accurately portrays the information in Figs. 1 and 2) to obtain input as to the source type. If the primary "angle ratio" was such that the source type was clearly defined, then the source type was recorded (labeled as "conclusion from table"). If the type was not clearly defined, the possible source types were recorded ("conclusion from table"). The question about whether or not a source type distinction was clearly defined was

based on the percentage difference between the "angle ratios" given in Table 1 [(a) and (b)] for the different source types at a particular frequency/mode combination. If the difference between the average "angle ratios" for different source types (based on the smaller of the two ratios) was less than 8%, then the source type was assumed not to be clearly defined. Thus with the 45˚/0˚ "angle ratios", each frequency/mode combination distinguishes only one source type from the other two, except for A_0 at 270 kHz, where all three can be distinguished. In contrast the 67.5˚/0˚ "angle ratios" distinguish all three source types for all of the frequency/mode combinations except for A_0 at 60 kHz. The arbitrary choice of 8% as the minimum value to distinguish between source types was based upon an examination of the percentage differences between the average "angle ratios" as given in table's 1(a) and 1(b). The lowest percentage differences between the average "angle ratios" of different source types were 3, 4.7, 6.5, 7.8 and 10.9%. Since the presence of noise would alter the "angle ratio" values, it was decided to use a minimum of an 8% difference to distinguish two different source types even though the noise-free "angle ratios" could successfully distinguish source types with smaller percentage differences.

In cases where the primary angle ratio did not uniquely define the source type, the WT peak magnitude of the secondary frequency/mode combination was determined in the zero-degree radiation direction. This magnitude was then divided into the WT peak magnitude of the same frequency/mode combination determined in the second radiation direction (either 45˚ or 67.5˚) to form a "secondary" angle ratio. This secondary angle ratio was then used with Table 1 (which corresponds to Figs. 1 through 4) to make the final determination of the source type. The results of the analysis by the "scheme" and a detailed example of the process of source-type determination are given in Appendix A and its associated tables A-1 and A-2. After examination of the results there (described in Appendix A), it was decided to focus on the effects of noise on source identification using the 45˚/0˚ angle ratio for the remainder of this research. The primary reason for this choice was due to the fact that the source identification "scheme" was not totally successful when the 67.5˚/0˚ angle ratios were used.

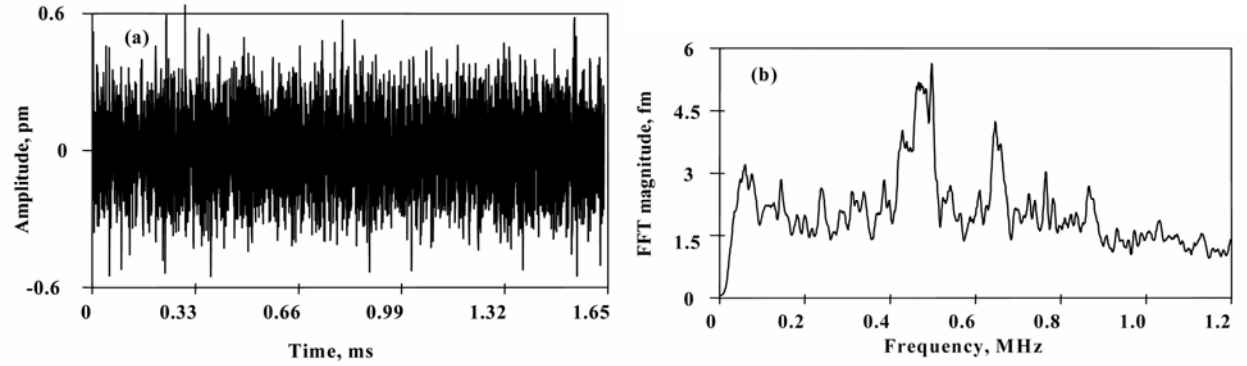

Fig. 10 Typical wideband experimental electronic noise (a) and FFT spectrum (b) showing the characteristics of the sensor/preamplifier system.

8. Description of Noise Signals

To make the study of the effect of electronic noise as realistic as possible, the noise signals were obtained from a wideband high-sensitivity sensor developed at NIST-Boulder [4, 5]. The noise signals were recorded with the sensor coupled only to air and protected by soft foam from any airborne signals. A total of ten noise signals were available. Each signal had been digitized by a 12-bit waveform recorder with a sampling interval of 0.1 μs/point. Each signal was about 16000 points in length, which resulted in the ten signals representing a total of about 16 ms of

noise. A typical time domain and fast Fourier transform (FFT) from one of these ten signals is shown in Fig. 10. This slightly smoothed FFT was calculated after the signals had been numerically bandpass-filtered (six-pole Butterworth) from 40 kHz to 1.2 MHz. This filter (applied to all the noise signals) was used to make the noise signals more representative of the frequency range of the FEM-modeled signals. After modifying the signal amplitudes (so they were less than the FEM signal amplitudes) and changing the units to picometers, the noise signals were examined to determine their consistency. First, the peak magnitudes for the 10 noise signals were determined. The mean peak magnitude was found to be 0.63 pm with a dispersion (mean value divided by the standard deviation) of 10% and a range of 0.54 to 0.73 pm. Thus the noise signals were considered to be relatively uniform in their peak signal magnitudes.

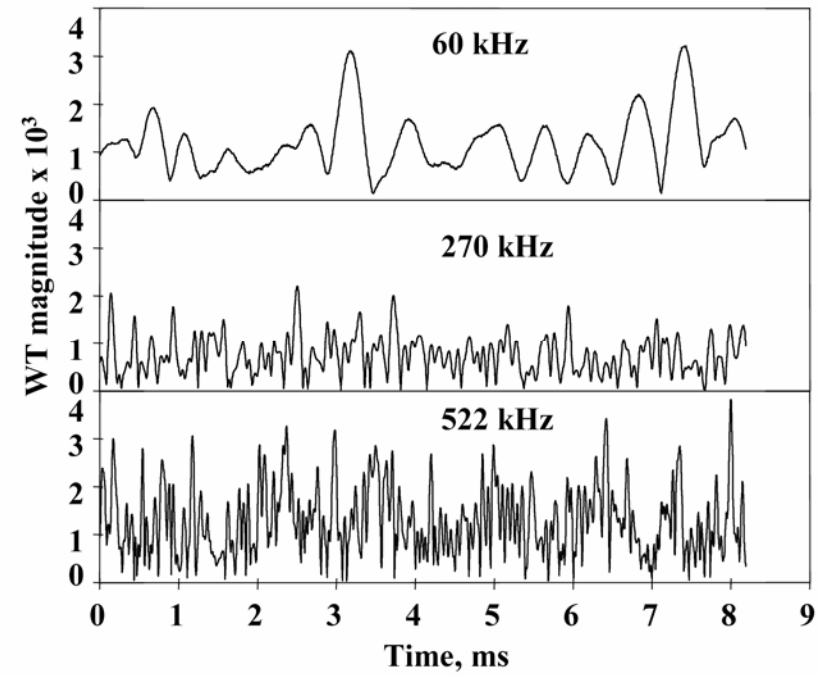

Fig. 11 WT magnitudes versus time showing the random changes of the electronic noise (8192 points) at the three key frequencies.

Before carrying out WTs on signal-plus-noise waveforms, some exploratory WTs were performed on the electronic noise signals. Since the WT software was limited to 8192 points, each noise signal was split into two equal parts. This resulted in 20 sub-signals. The WT computations used the same parameters as for the FEM-based signals except that the number of points was increased to 8192 to match the length of the 20 sub-signals. Then plots of WT magnitude versus time at each of the three key frequencies were obtained. Figure 11 shows results for one sub-signal. It is clear from this figure that the WT magnitude versus time varies over a wide range for each of the three key frequencies. Comparisons of these results with those from the other sub-signals showed differing variations of WT magnitudes with time. Also, the number of fluctuations of the WT magnitudes increases with increasing frequency (likely a characteristic of the WT used in this research). Further, the WT magnitude variations in Fig. 11 imply that when noise is added to the FEM-generated AE signals, the WT peak magnitudes of the signal plus noise (S+N) could experience noise-induced modification. It might also be expected that in a particular S+N case the noise-induced changes in WT peak magnitudes would likely depend on the noise characteristics near the times where the noise-free AE signals have peak WT magnitudes (at the key frequencies) that represent the arrivals of the fundamental Lamb modes. Since,

for real-world AE signals, the amplitudes and frequencies of the underlying noise signal at the times of mode arrivals would be a random and unpredictable condition, it was concluded that a statistical study of noise effects would be necessary.

9. Creation of Modeled AE Signals with Noise

To form a suitable noise database for a statistical study, the modified database of ten noise signals was divided into a total of 100 different segments, each nominally 160 μs in length. The S+N database was then constructed for particular cases (source type and depth) of interest. One noise signal was added to the FEM-based (noise-free) AE signal from a radiation angle of zero degrees, and another was added to the signal for the 45˚ radiation angle. Thus a pair of noise-modified signals was obtained. Before adding the noise signals they were multiplied by a *factor* to obtain a certain S/N ratio. The "overall" S/N ratio was based on the peak amplitude of the noise-free FEM signal divided by the result of the same *factor* times the mean peak amplitude (0.63 pm, given above) representative of all the noise signals. The overall S/N ratio was also based on the noise-free AE signal's peak amplitude in the zero-degree radiation direction. Thus, since the same *factor* was used to prepare each noise signal for addition to the 45-degree FEM-based AE signal, the real S/N ratio in that direction was actually less. The decrease in the S/N ratio in this direction depends on the loss of peak AE signal amplitude with radiation direction for the particular source type and source depth. This loss of noise-free signal-peak amplitude as a function of the radiation angle and the source depth is shown in Figs. 12, 13 and 14. The loss is considerable for the in-plane dipole and more moderate for the other two source types (smallest for the shear source). This strategy of using different noise signals for the zero- and 45-degree FEM-based signals corresponds to real AE testing, where there is no direct relationship between the electronic noise at one sensor versus another. Thus, pairs (0˚ and 45˚) of S+N signals were prepared using the same noise-free FEM signals and different noise signals. A total of 50 pairs was created for each overall S/N ratio that was studied for the chosen source types and depths. These 50 signals were called a "set" of S+N signals for a given case. In order to be able to directly track the effects of different "overall" S/N ratios applied to the same pair (zero and 45 degrees, FEM based for a given case) of noise-free signals, the same sequence of noise pairs (multiplied by a different *factor* to create a different "overall" S/N ratio) was added respectively to the 0˚ and 45˚ pairs to form a new set of S+N signals. In summary, 100 noise segments were combined with the same 0˚ and 45˚ (FEM, noise-free signals) to form the S+N signal database set at each overall S/N ratio.

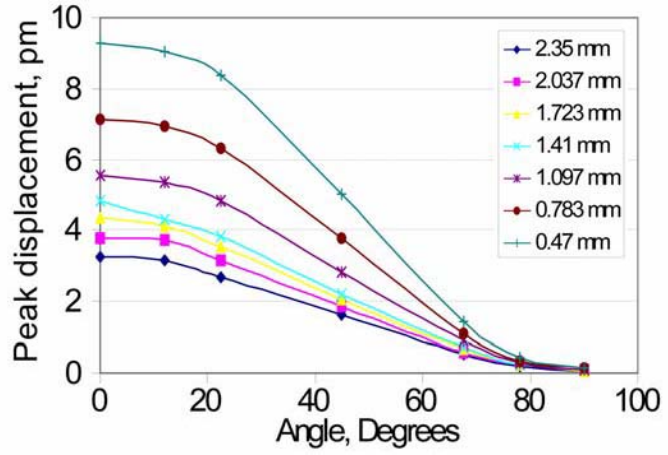

Fig. 12 Peak noise-free signal amplitude versus radiation angle at 180 mm propagation distance for in-plane dipole source.

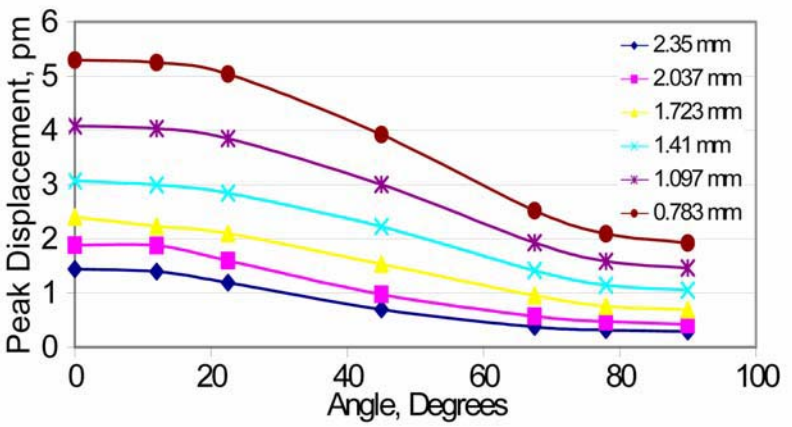

Fig. 13 Peak noise-free signal amplitude versus radiation angle at 180 mm propagation distance for microcrack initiation source

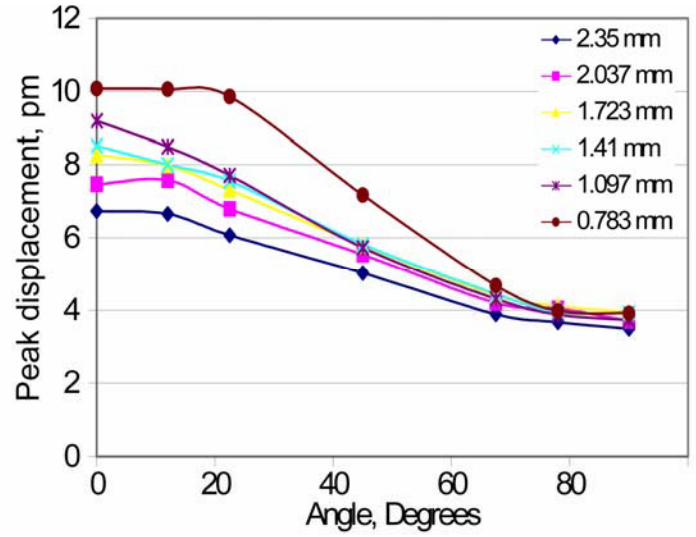

Fig. 14 Peak noise-free signal amplitude versus radiation angle for balanced shear source at 45 degrees about the y-axis and at 180 mm propagation distance

The "effective" S/N ratio for source-type distinctions is really determined by the WT peak magnitude representing a mode arrival at that frequency compared to the WT magnitudes of the noise signal around the time of the mode arrival. But since the noise WTs have considerable variation, it is not possible to compute these effective S/N ratios. It is possible to point out when the AE noise-free WT peak magnitude will be the smallest. On the average, when the AE noise-free WT peak magnitude is the smallest, the effective S/N will be the smallest. Thus, the poorest effective S/N ratio will be for the 45˚ radiation direction when it is necessary to use a secondary frequency to complete the source identification scheme. The noise-free WT peak magnitudes in this situation are essentially twice reduced in magnitude compared to the 0˚ primary-frequency peak WT magnitude. The first reduction is that due to the use of the secondary-frequency WT peak magnitudes, and the second reduction is due to the use of peak WTs from the 45˚ signal to form the secondary ratio. These reductions are shown by the "reduction factor" in tables A-1. If only a primary angle ratio was necessary, then as shown in the last column (reduction factor) of table A-1, the loss of peak WT magnitude was not as great. In all cases it is expected that the effective S/N ratio (primary or if it is required for unique source identification, the secondary) for the 45˚ direction will most often control the accuracy of the source identification results.

10. Lowest S/N ratios for High-Probability Correct Source Identification of the Three Source Types

The cases (source type and depth) most likely to require the largest overall S/N ratio to correctly identify most of the AE S+N signals are those where an angle ratio based on the secondary frequency is necessary, so the research was focused on cases of that type. These cases can be identified in table A-1 as those with the largest reduction factor shown in the last column of the table. Since for certain source types and depths only a 45˚/0˚ primary angle ratio was required, some of those cases were examined as well. The selection of particular cases also covered a variety of the combinations of modes and frequencies that appear in table A-1. The final selections for full statistical analysis were as follows: (i) shear at 0.783 mm depth with primary angle ratio from A_0 at 60 kHz, secondary angle ratio from A_0 at 270 kHz, and a reduction factor of 5; (ii) in-plane dipole at 1.723 mm depth with primary angle ratio from A_0 at 60 kHz, no required secondary angle ratio, and a reduction factor of 2; (iii) microcrack initiation at 1.41 mm depth with primary angle ratio from A_0 at 60 kHz, secondary angle ratio from A_0 at 270 kHz, and a reduction factor of 4.7; (iv) in-plane dipole at 2.35 mm depth with primary angle ratio from S_0 at 522 kHz, secondary angle ratio from S_0 at 270 kHz, and a reduction factor of 5.1; and (v) shear at 2.037 mm depth with primary angle ratio from S_0 at 522 kHz, no required secondary angle ratio, and a reduction factor of 1.4.

The first analysis of the set of data for a particular case of source type and source depth is described here in detail. We believe the detailed description is necessary to provide the reader with a fuller understanding of the complications caused by changes in modal amplitudes due to noise. For subsequent cases, the focus will be on the statistical results of correct source identification for the 50 different pairs of S+N signals making up the set at a particular overall S/N ratio. For the first analysis, a shear source at a depth of 0.783 mm [(ii) above] was selected. As can be seen from table A-1(b) the identification of this source requires use of both a primary and secondary angle ratio.

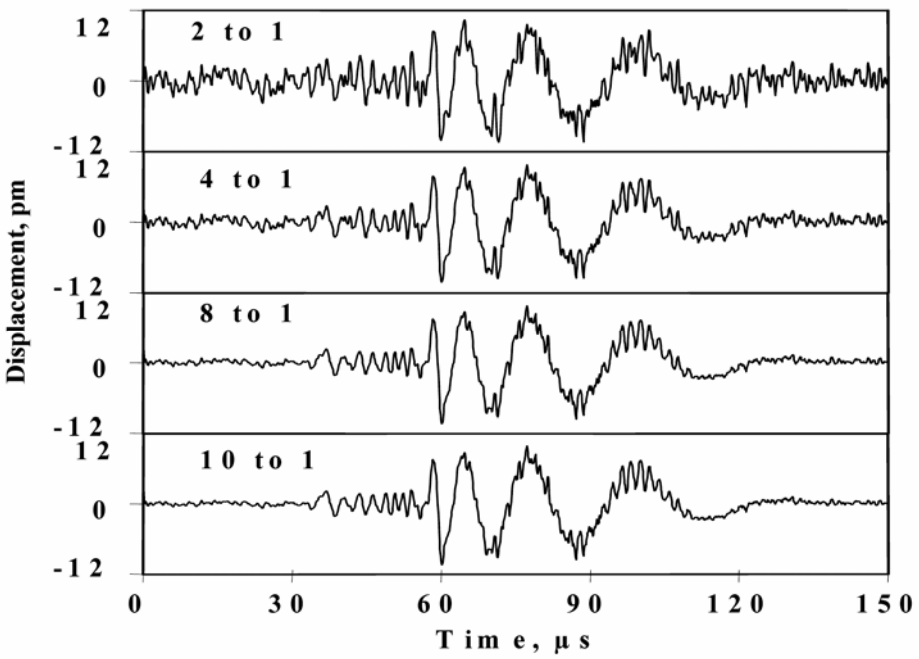

Fig. 15 Typical signals for zero degree radiation direction at various overall S/N ratios for balanced shear source at 180 mm propagation distance and a depth of 0.783 mm.

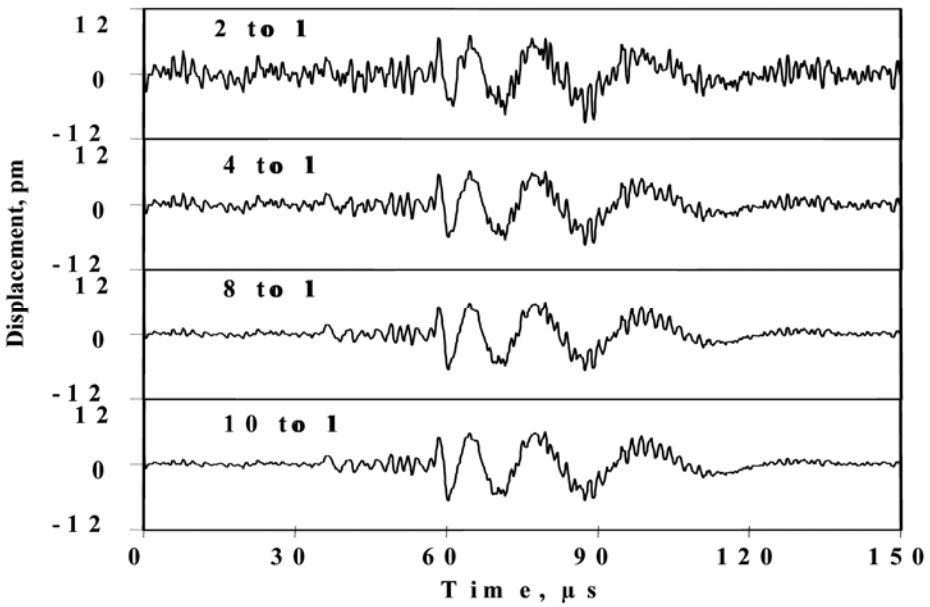

Fig. 16 Typical signals for 45- degree radiation direction at the same various overall S/N ratios for balanced shear source at 180 mm propagation distance and a depth of 0.783 mm.

Figures 15 and 16 show some typical S+N waveforms at different S/N ratios for this case. Figure 15, for the 0˚ direction, indicates even at an S/N ratio of 4 to 1 that the first portion of the AE signal can be seen. At higher S/N ratios the early portion (extensional mode) of the AE signal can be seen even more clearly. The lower "actual" S/N ratio in the 45˚ direction is demonstrated in Fig. 16 at the same overall S/N ratios. The actual S/N ratios are less here, since, for example, at an overall S/N ratio of 2 to 1, the actual S/N ratio in this direction is 1.3 to 1.

Before turning to statistical results for the above shear source (at particular overall S/N ratios), it is instructive to look at the typical plots of WT magnitudes versus time (from which the peak magnitudes are extracted) that are required to identify this source at a particular S/N ratio. It is most insightful to examine the WT magnitudes versus time separately for the noise-free AE signals and the noise signals. As table A-1(c) shows, there are actually four noise-free WT curves (from the 0˚ and 45˚ propagation directions, with WTs at both 60 and 270 kHz) to consider along with the two noise-only curves used to build the S+N signals. Thus Fig. 17(a) shows (top) the WT magnitudes versus time from the 0˚ direction noise-free signal for the primary frequency (A_0 at 60 kHz). This figure also shows (bottom) with the same WT-magnitude scale a WT magnitude versus time at this frequency from a typical noise signal. Similarly part (b) shows at the primary frequency the WT magnitude versus time for the 45˚ direction noise-free signal and a different typical noise signal. The amplitude of the noise signals for these figures was based on an overall S/N ratio of 2 to 1 for the 0˚ direction. In a similar fashion, Fig. 18 shows the same type of results for the secondary frequency (A_0 at 270 kHz), where the two noise signals were the same ones used for Fig. 17. Since the WT magnitude scales are the same for both the noise-free signal and noise in each case, these figures directly show the potential for greater impact of noise on the WT-based secondary angle ratios when they are necessary for source identification. Clearly, based on WT magnitude results for the secondary frequency, the noise-free signals are not as dominant relative to the WTs of the typical noise signals as the primary frequency WT magnitude results are. This statement is particularly true for the secondary frequency at the 45˚ radiation angle. It should be noted that the WTs of S+N signals are not the linear sum of the WT of the noise-free signal plus the WT of the noise.

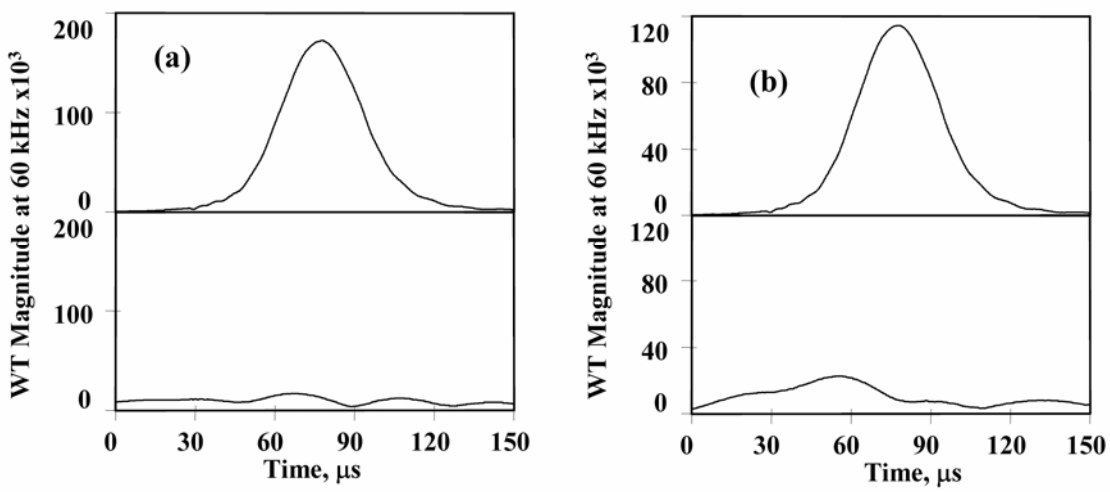

Fig. 17 WT magnitude versus time for primary frequency (60 kHz/A_0) at (a) zero-degree radiation angle and (b) 45-degree radiation angle. Top is for the noise-free shear AE signal at 0.783 mm depth and 180 mm propagation distance. Bottom is for typical noise added to the AE signal for an overall S/N ratio of 2 to 1.

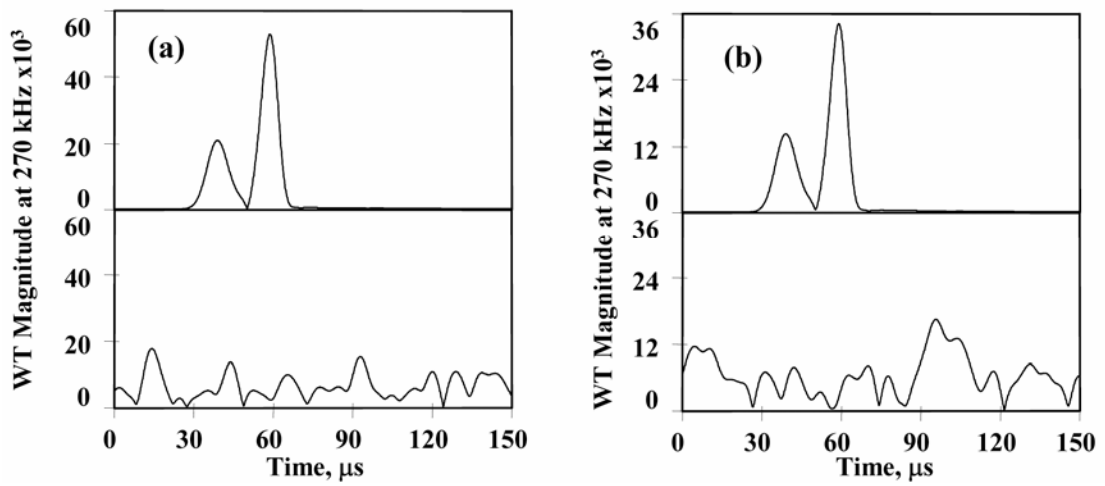

Fig. 18 WT magnitude versus time for secondary frequency (270 kHz/A_0) at (a) zero-degree radiation angle and (b) 45-degree radiation angle. Top is for the noise-free shear AE signal at 0.783 mm dept and 180 mm propagation distance. Bottom is for typical noise added to the AE signal for an overall S/N ratio of 2 to 1.

To generate the statistical results for this shear case, the primary and secondary angle ratios were determined for all 50 pairs of S+N signals in each set at different overall S/N ratios. Figure 19 shows the percentage of correct source-type determinations as a function of the overall S/N ratio (defined by the 0˚ direction) for the shear case. This figure shows the percentage of correct identification choices based on the primary WT peak-magnitude angle ratio, the corresponding results based on the secondary WT peak-magnitude angle ratio, and the total percentage of correct identifications (when neither the primary nor the secondary angle ratio resulted in an identification error). In these and subsequent similar results, the decision about whether a source determination was in error was based on the arbitrary assumption that incorrect results would be obtained if the calculated angle ratio for the S+N data was more than ±10% from the average no-noise value for the correct source type. The choice of ±10% is fairly conservative in that the

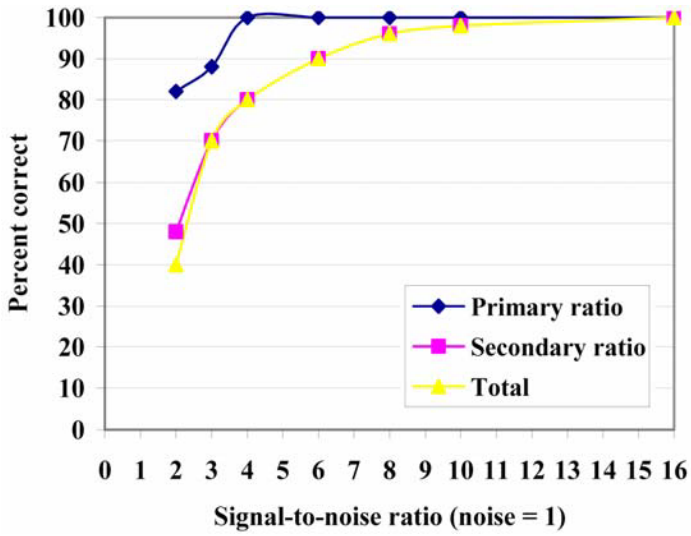

Fig. 19 Percent of trials out of 50 with correct source identification for balanced shear at 45 degrees about the y axis and 0.783 mm depth.

typical differences in table A-1 between correct or incorrect source choices are on average about 32 %. But a close examination of all the percentage differences in table A-1 shows that there are four cases where a 10% difference in the right direction would likely result in the selection of an incorrect source type. These cases, along with the ratio percentage difference to the next nearest and incorrect source type, are: (i) balanced shear at a depth of 0.783 mm with a +9.2% difference for the secondary-angle ratio, and (ii) microcrack initiation at depths of 1.41, 1.097 and 0.783 mm with respective secondary angle-ratio differences of -11%, -9.9% and -11%. In these cases, the choice ±10% is not conservative in the direction towards the next nearest source type. An allowed difference of about ±5% would be conservative in these cases. In spite of this observation, the decision was made to use ±10% so that the allowed percentage variation used as the basis for judging correct source identification would always be the same for this initial study. Thus, in some cases, the ±10% overestimates the number of errors in source identification, while in other cases, it underestimates the number of errors. A future study could develop a more complicated approach to potentially deal with this issue. It is clear from Fig. 19 that the total percentage of errors is dominated by errors in the secondary ratio at S/N ratios where the correct identification is made about 50 % or more of the time.

We next describe how this ±10% process was implemented for the shear case to obtain the results in Fig. 19. The primary frequency/mode was A_0 at 60 kHz. Table 1(a) gives the no-noise average angle ratio for this shear source type at 0.66. Thus, this primary angle ratio eliminates the in-plane dipole (average no-noise angle ratio of 0.50) source. But the source could still be either a microcrack (average no-noise angle ratio of 0.68) or a shear (average no-noise angle ratio of 0.66). With the adopted criteria that ratio errors must be ±10% or less, the ratio when noise is present must be between 0.59 and 0.73 to result in a correct source-type decision. This criterion was used, even though in the current case an unlimited range of angle ratios above 0.66 would not result in incorrect source-type decision. Thus, when a signal with noise had a primary angle ratio within the above range (0.50 to 0.73) the correct decision was that the source was either a microcrack or shear source.

Since the primary angle ratio did not uniquely identify the source type in this detailed case, a secondary ratio was required for unique identification. The secondary angle ratio, in this case, comes from A_0 at 270 kHz [see table A-1(c)]. Table 1(a) shows that a no-noise average ratio of

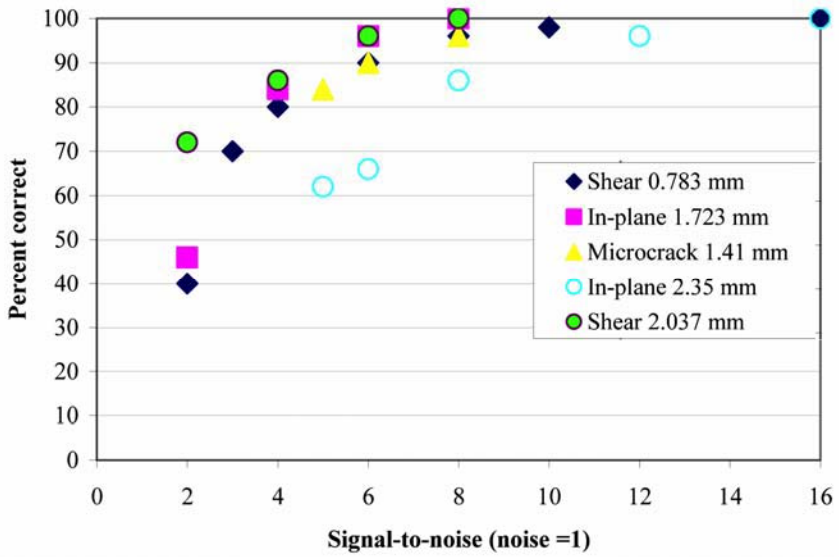

Fig. 20 Percent of trials out of 50 with total correct source identification versus S/N ratio for all cases studied.

0.64 distinguishes a shear source from a microcrack source (no-noise ratio of 0.71). To be correct (±10 %), the angle ratio when noise is present must be between 0.58 through 0.70. It should be noted that at this point the use of ±10 % is problematic for this case, since 0.70 is too close to the no-noise value of 0.71 for the incorrect microcrack source. This potential problem is ignored in this work as was discussed above.

Figure 20 shows the percentage of total correct identifications versus the overall S/N ratio for all the cases (a source type and depth) studied in detail. Again, for Fig. 20, an incorrect result occurs if either or both the primary and/or secondary angle ratios gave an incorrect source type (a ratio more than ±10% from the no-noise average ratio of the correct source type).

11. Discussion of Results on Percentage of Correct Source Identifications in the Presence of Electronic Noise

Figure 20 shows in general that a relatively high overall S/N ratio is required to obtain proper source identification approximately 90% of the time. But this figure also shows some variation in the minimum S/N ratio required to reach the approximately 90% correct result. There seems to be at least two factors that lead to this variation. First, changes in the amount of decrease in the peak WT magnitudes at 45˚ compared to the 0˚ magnitudes as a function of source type and depth. This change, as was discussed earlier, is greatest for the in-plane dipole source and is more moderate for the other two sources types. Second, when a secondary angle ratio is required to obtain unique source identification, there is the additional drop in the secondary WT peak magnitudes compared to the primary WT peak magnitudes.

We have seen that many factors enter into a decision as to what overall S/N ratio is necessary obtain the correct source type approximately 90% of the time. Because of this a simple conclusion of the required S/N ratio cannot be made. In a multi-source environment, where all three of the source types examined in this study are present, the typical choice would be to assume that an overall S/N ratio of about 6 to 1 would be required to identify the correct source type approximate 90% of the time. But as Fig. 20 shows the in-plane dipole case at a depth of 2.35 mm re-

quires a S/N ratio of more than 8 to 1 to obtain about a 90% rate of correct source identification. In spite of extensive efforts, a reason for this difference could not be determined.

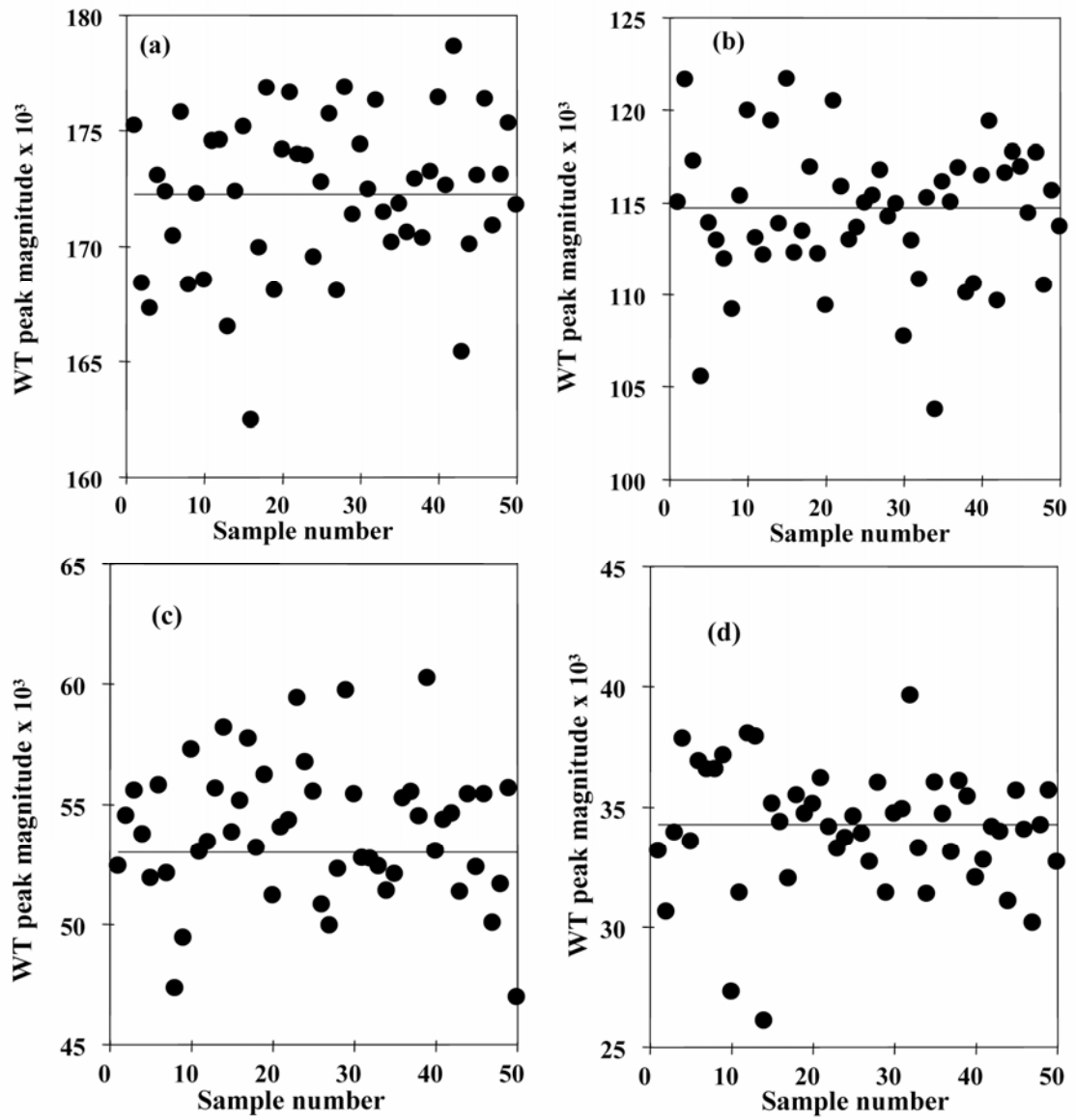

Fig. 21 WT peak magnitudes for the 50 samples at a S/N ratio of 4 to 1 for balanced shear source at a depth of 0.783 mm: (a) 60 kHz and zero-degree direction; (b) 60 kHz and 45-degree direction; (c) 270 kHz and zero-degree direction; (d) 270 kHz and 45-degree direction.

For signals with smaller overall S/N ratios, the source identification procedure could still be carried out. In such cases, the identified source could be flagged as questionable. Alternatively, for experiments where a group of sensors are all located in an array about AE sources that all originate from the same location such as the tip of a crack, more than one sensor's data could be used at the two angles (zero and 45 degrees). For example, if two sensors were located at each angle (a total of four sensors is not unlikely in an experimental setup) then several primary and secondary angle ratios could be formed to determine the likely source type. The four possible ratios are for data at the angles of $45_1/0_1$, $45_1/0_2$, $45_2/0_1$ and $45_2/0_2$, where the subscripts 1 and 2 refer to sensors 1 and 2 at each radiation angle. Thus potentially four different determinations of

the source type could be made. Due to the random variations in the noise, it is possible that the source type that occurs most frequently is the actual source type. An additional study would be necessary to predict the probability of determining the correct source type by the use of such data.

Table 2 Statistical results of WT peak magnitudes for S+N shear case at 0.783 mm depth compared to no-noise values (from data shown in Fig. 21).

		Statistical results for 50 trials of S+N at S/N ratio of 4 to 1		
Frequency (kHz) and propagation direction (deg.)	No-noise WT peak magnitude	Mean WT peak magnitude	Difference no-noise to mean WT peaks (%)	Dispersion of the mean WT peak magnitude (%)
60 at 0	172274	172262	0.01	1.9
60 at 45	114727	114298	0.4	3.3
270 at 0	53006	53877	2	5.3
270 at 45	34273	34114	0.4	7.5

Further analysis of the results generated in the examination of the S+N sets of data confirms some of the expectations that have been discussed earlier. Figure 21(a) shows the typical scatter in the magnitude of the WT peak for the 0˚ radiation direction at 60 kHz for the shear case at a depth of 0.783 mm. This scatter was determined from a data set with the overall S/N ratio at 4 to 1. Statistical analysis of the WT peak values resulted in a mean value of 172300 with a dispersion of 1.9%. The mean value is within 0.01 % of the no-noise value that is shown in Fig. 21(a) as a straight line. In Figs. 21(b) to 21(d) similar results are shown for the other WT magnitudes necessary for unique source identification in this case. These figures show that the WT peak magnitudes scatter in a random fashion both above and below the no-noise value. Table 2 shows the mean values and their dispersions for all four figures [WT peak magnitudes of the 60 kHz primary frequency at 0˚ and 45˚ (radiation angles) and the same results for the 270 kHz secondary frequency, which was necessary for unique source identification]. The results in the table show that the dispersion increases from a minimum for the primary frequency at the 0˚ radiation angle to the expected maximum at the secondary frequency at the 45˚ radiation angle. The dispersion values in this table also indicate that the noise-based errors in the primary and secondary angle ratios depend primarily on the errors in the WT peak magnitudes in the 45˚ directions, since the 45˚ dispersion value is always greater than the 0˚ direction results at the same frequency. And further, the table shows that the secondary angle ratios will typically control the accuracy of source identification since these dispersions are higher. These results are consistent with those shown in Figs. 17 through 21.

Ideally, it may be possible that a filtering technique could be developed that would improve S/N ratios and thus allow correct sources types to be determined more often at lower S/N ratios. The development of such a filtering scheme is not an easy task. The primary reason is because electronic noise also inhabits the three key frequency bands where the energetic modes of the AE noise-free signal are present. Thus, it may be difficult to selectively reduce the electronic noise without significantly changing the important parts of the AE signal that will be used to identify the source.

In the application of this research study to real experimental data, a question needs to be answered. Given a S/N ratio determined from the ratio of the peak of the S+N to the typical electronic noise, is this ratio close to the overall S/N ratio used in this study where the AE source-based signal was available without noise? Take for example a typical set (microcrack initiation at a depth of 1.41 mm) of 50 S+N waveforms used in this study at an overall S/N ratio of 6 to 1 (where likely the correct source type is determined about 90% of the time). Examination showed that for this example the range of the S+N to N ratios was from about 5.8 to 1 to 6.6 to 1. Also, the mean ratio was 6.2 to 1 with a dispersion of 3%. Thus, at overall S/N ratios where correct source identification is likely about 90% of the time, the overall S/N ratio used in this study is not much different from the S+N to N ratio that can be measured in experimental cases.

12. Conclusions

The following conclusions apply to the results for the 4.7 mm thick aluminum plate and the experimental wideband electronic noise. For other materials and/or plate thicknesses, appropriate changes in key frequencies and associated modes will be necessary. These changes could likely be predicted using modeled acoustic emission (AE) signals.

- A total of three different factors were found to result in attenuation of the AE signals and their wavelet transform (WT) magnitudes needed for the source identification scheme. These are: (1) loss as the radiation angle increases from 0˚ to 90˚; (2) decrease in amplitude of the A_0 mode at depths near the plate midplane and of the S_0 mode near the plate surface; and (3) need for both a primary and secondary (which is based on lower-amplitude portions of the source-based signal) "angle ratio" for complete source identification in some cases (a case is a source type and depth).
- After considering the above attenuation factors, it was concluded that the effects of electronic noise on the accuracy of source identification could best be examined by considering a particular ratio of WT peak magnitudes at two angles. The ratio used was for the 45˚/0˚ angles.
- Due to time-based random variations in the WTs of the electronic noise signals, it was necessary to do a statistical study of the effects of noise on correct source identification.
- To assure that the correct AE source type could be correctly identified approximately 90% of the time (from among the three source types under study in this report) typically an overall S/N ratio of at least 6 to 1 is required. This result implies that all source identification approaches (not just the one used on this research) that depend on Lamb-wave modal magnitudes will require large S/N ratios to be successful. The results also indicate that the modal magnitudes that are used in an identification approach should be those from the large modal magnitudes (e.g., using 0˚ radiation angles where possible) since these magnitudes will be less subject to noise-induced errors.
- The current database of S+N signals is ideal to use both to develop and check the accuracy of various noise-reduction approaches, since the original noise-free signal is available.

Acknowledgement

This work was partially supported by NASA Langley Research Center. We also acknowledge the original development of the finite element code by John Gary (retired) of NIST, Boulder, Colorado. We wish to express our gratitude to Prof. M. Takemoto, who released the source code of the wavelet transform that his group had developed; this wavelet transform source code was utilized in the creation of the AGU-Vallen Wavelet software. We also thank Dr. Y. Mizutani and Mr. Jochen Vallen for making the AGU-Vallen Wavelet software into a highly usable form. The contributions of all the above people have significantly advanced the field of acoustic emission.

References

1. M.A. Hamstad, K.S. Downs, and A.O'Gallagher, "Wavelet Transform Signal Processing to Distinguish Different Acoustic Emission Sources," Journal of Acoustic Emission, 2003, **21**, 52-69.
2. Vallen-Systeme GmbH, Münich, Germany, http://www.vallen.de/wavelet/index.html, 2001, software version R2002.0703.
3. M.A. Hamstad, K.S. Downs and A. O'Gallagher, "Practical Aspects of Acoustic Emission Source Location by a Wavelet Transform," Journal of Acoustic Emission, 2003, **21**, 70-94, A1-A7.

4. M.A. Hamstad and C.M. Fortunko, "Development of Practical Wideband High Fidelity Acoustic Emission Sensors," Nondestructive Evaluation of Aging Bridges and Highways, Steve Chase, Editor, Proc. SPIE 2456, 1995, pp. 281-288.

5. M.A. Hamstad, "Improved Signal-to-Noise Wideband Acoustic/Ultrasonic Contact Displacement Sensors for Wood and Polymers," Wood and Fiber Science, **29** (3), 1997, pp. 239-248.

For Appendix, see 22-A01.

Appendix A: Details of the Application of the Source Identification Scheme

M. A. Hamstad and A. O'Gallagher

The 19 signals in the database (three source types at six or seven depths each) were analyzed according to the scheme described in section eight. The analysis was done for both the 45/0 and 67.5/0˚ angle ratios. Table A-1 outlines the key results for each case (a source type and source depth defined a case) of the three-source-type database when 45˚ was the second radiation angle. In this table the logic of the analysis scheme outlined in section eight flows from left to right. The first column identifies the known source type. The scheme and calculations proceed starting from the third column as if the source type was unknown. The next-to-last column shows the source type that was "determined" for comparison with the known information. Table A-2 gives the same results for the choice of 67.5˚ for the second angle. The last column (called the "reduction factor") in each of these tables records the ratio of the peak WT magnitude of the primary frequency from the zero degree direction divided by the peak WT magnitude of the lowest peak magnitude at the second angle (primary or secondary as required) to uniquely determine the source type. The tables also record the percentage difference from the calculated primary and as needed secondary angle ratios for each signal case as compared to the average angle ratios (table 1) from the nearest source type(s) eliminated at each step.

At first glance, a comparison of the two tables seems to indicate that the choice of 67.5˚ as the second angle would be best. The reason for this tentative conclusion is that the percentage differences between the angle ratios for the selected source(s) versus the angle ratios for the source(s) rejected for a given case is considerably greater in the 67.5˚ case. Thus with this second angle, errors in angle ratio values due to the effects of the presence of noise might be expected to be less likely to lead to incorrect selection or rejection of source types. But upon closer examination, there are several reasons why the choice of 45˚ seems to be better. First, the last column (reduction factor) in the two tables indicates that for most of the depths of the in-plane dipole source, the loss in the WT peak magnitudes at 67.5˚ [table A-2(a)] for the lowest peak WT magnitude required for unique source identification is considerably greater than that for 45˚ [table A-1(a)]. Thus the advantage of potential tolerance to angle ratio errors could be overpowered by a substantial increase in the size of the noise-induced errors because of a considerably lower S/N ratio at 67.5˚. Second, when the two tables [A-1(c) and A-2(c)] are compared for the microcrack initiation source, there are problems of a different type. In certain cases (depths of 2.35 to 1.723 mm) the frequency/mode combination at 67.5˚ is not the same as that at zero degrees for either the primary and/or the secondary angle ratio. Thus a relevant angle ratio could not be determined, and it was not possible to identify the source type using the scheme described in section eight. For the shear source, a comparison of the two tables [A-1(b) and A-2(b)] does show a genuine opportunity to experience reduced effects from errors in peak WT magnitudes caused by noise if the 67.5˚angle is used for most depths (except 1.097 and 0.783 mm). The reason for the potential advantage is that the WT mode peak magnitudes decrease only moderately between 45˚ and 67.5˚, while the difference in the average angle ratio value between alternate source type(s) selections has increased markedly. This potential advantage for the shear source type is outweighed by the potential difficulties of the other two sources types. Further, the practicality of implementing angle ratios at different angles for different source types does not make sense when the problem is to identify *unknown* source types. Thus, the 45/0˚ angle ratio was used in the signal-plus-noise considerations in this paper.

Table A-1(a) Source identification process using ratios of WT peak magnitude ratio of 45˚/0˚ for in-plane dipole source

Source type	Depth (mm)	Primary freq. (kHz/mode)	Primary angle ratio	Table to consult	Conclusion from table	Percentage difference to next nearest source type	Secondary mode/freq. (kHz)	Secondary angle ratio	Table to consult	Conclusion from table	Percentage difference to next nearest source type	Final conclusion	Reduction factor = (Highest 0˚)/(lowest 45˚ peak)
In-plane dipole	2.35	$522/S_0$	0.49	2(a)	Either in-plane dipole or microcrack	51	$270/S_0$	0.5	2(a)	In-plane dipole	28	In-plane dipole	5.1
In-plane dipole	2.037	$522/S_0$	0.49	2(a)	Either in-plane dipole or microcrack	51	$60/A_0$	0.5	2(a)	In-plane dipole	36	In-plane dipole	3.3
In-plane dipole	1.723	$60/A_0$	0.5	2(a)	In-plane dipole	32	NA	NA	NA	NA	NA	In-plane dipole	2
In-plane dipole	1.41	$60/A_0$	0.5	2(a)	In-plane dipole	32	NA	NA	NA	NA	NA	In-plane dipole	2
In-plane dipole	1.097	$60/A_0$	0.5	2(a)	In-plane dipole	32	NA	NA	NA	NA	NA	In-plane dipole	2
In-plane dipole	0.783	$60/A_0$	0.5	2(a)	In-plane dipole	32	NA	NA	NA	NA	NA	In-plane dipole	2
In-plane dipole	0.47	$60/A_0$	0.5	2(a)	In-plane dipole	32	NA	NA	NA	NA	NA	In-plane dipole	2

Table A-1(b) Source identification process using ratios of WT peak magnitude ratio of 45˚/0˚ for shear at 45˚ about y-axis source

Source type	Depth (mm)	Primary freq. (kHz/mode)	Primary angle ratio	Table to consult	Conclusion from table	Percentage difference to next nearest source type	Secondary mode/freq. (kHz)	Secondary angle ratio	Table to consult	Conclusion from table	Percentage difference to next nearest source type	Final conclusion	Reduction factor = (Highest 0˚ peak)/(lowest 45˚ peak)
Shear	2.35	$522/S_0$	0.74	2(a)	Shear	34	NA	NA	NA	NA	NA	Shear	1.4
Shear	2.037	$522/S_0$	0.74	2(a)	Shear	34	NA	NA	NA	NA	NA	Shear	1.4
Shear	1.723	$522/S_0$	0.74	2(a)	Shear	34	NA	NA	NA	NA	NA	Shear	1.4
Shear	1.41	$60/A_0$	0.66	2(a)	Shear or microcrack	24	$522/S_0$	0.74	2(a)	Shear	38	Shear	2.2
Shear	1.097	$60/A_0$	0.67	2(a)	Shear or microcrack	25	$522/S_0$	0.75	2(a)	Shear	39	Shear	3.8
Shear	0.783	$60/A_0$	0.67	2(a)	Shear or microcrack	25	$270/A_0$	0.65	2(a)	Shear	9.2	Shear	5

Table A-1(c) Source identification process using ratios of WT peak magnitude ratio of 45˚/0˚ for microcrack initiation source

Sour-ce type	Depth (mm)	Primary freq. (kHz /mode)	Pri-mary angle ratio	Table to consult	Conclusion from table	Percent. difference to next nearest source type	Second-ary mode /freq. (kHz)	Second-ary angle ratio	Table to consult	Conclusion from table	Percent. Differ-ence to next nearest source type	Final conclu-sion	Reduction factor = (Highest 0˚) /(lowest 45˚ peak)
Micro -crack	2.35	522/S_0	0.47	2(a)	In-plane dipole or microcrack	57	270/S_0	0.64	2(a)	Micro-crack	22	Micro-crack	2.7
Micro -crack	2.037	60/A_0	0.68	2(a)	Shear or microcrack	27	522/S_0	0.46	2(a)	Micro-crack	61	Micro-crack	2.2
Micro -crack	1.723	60/A_0	0.68	2(a)	Shear or microcrack	27	522/S_0	0.46	2(a)	Micro-crack	61	Micro-crack	4.9
Micro -crack	1.41	60/A_0	0.68	2(a)	Shear or microcrack	27	270/A_0	0.72	2(a)	Micro-crack	11	Micro-crack	4.7
Micro -crack	1.097	60/A_0	0.71	2(a)	Shear or microcrack	30	270/A_0	0.71	2(a)	Micro-crack	9.9	Micro-crack	4.4
Micro -crack	0.783	60/A_0	0.68	2(a)	Shear or microcrack	27	270/A_0	0.72	2(a)	Micro-crack	11	Micro-crack	4.1

Table A-2(a) Source identification process using ratios of WT peak magnitude ratio of 67.5˚/0˚ for in-plane dipole source

Source type	Depth (mm)	Primary freq. (kHz /mode)	Primary angle ratio	Table to consult	Conclusion from table	Percent. diff. to next nearest source type	Second. mode /freq. (kHz)	Secondary angle ratio	Table to consult	Conclusion from table	Percent. diff. to next nearest source type	Final conclusion	Reduction factor = (Highest 0˚)/ (lowest 45˚ peak)
In-plane dipole	2.35	$522/S_0$	0.15	2(b)	In-plane dipole	40	NA	NA	NA	NA	NA	In-plane dipole	6.6
In-plane dipole	2.037	$522/S_0$	0.15	2(b)	In-plane dipole	40	NA	NA	NA	NA	NA	In-plane dipole	6.6
In-plane dipole	1.723	$60/A_0$	0.15	2(b)	In-plane dipole	187	NA	NA	NA	NA	NA	In-plane dipole	6.8
In-plane dipole	1.41	$60/A_0$	0.15	2(b)	In-plane dipole	187	NA	NA	NA	NA	NA	In-plane dipole	6.8
In-plane dipole	1.097	$60/A_0$	0.15	2(b)	In-plane dipole	187	NA	NA	NA	NA	NA	In-plane dipole	6.8
In-plane dipole	0.783	$60/A_0$	0.15	2(b)	In-plane dipole	187	NA	NA	NA	NA	NA	In-plane dipole	6.8
In-plane dipole	0.47	$60/A_0$	0.15	2(b)	In-plane dipole	187	NA	NA	NA	NA	NA	In-plane dipole	6.8

Table A-2(b) Source identification process using ratios of WT peak magnitude ratio of 67.5˚/0˚ for shear at 45˚ about y-axis source

Source type	Depth (mm)	Primary freq. (kHz /mode)	Primary angle ratio	Table to consult	Conclusion from table	Percent. diff. to next nearest source type	Secondary mode/freq. (kHz)	Secondary angle ratio	Table to consult	Conclusion from table	Percentage difference to next nearest source type	Final conclusion	Reduction factor = (Highest 0˚)/(lowest 45˚ peak)
Shear	2.35	$522/S_0$	0.58	2(b)	Shear	74	NA	NA	NA	NA	NA	Shear	1.7
Shear	2.037	$522/S_0$	0.58	2(b)	Shear	74	NA	NA	NA	NA	NA	Shear	1.7
Shear	1.723	$522/S_0$	0.58	2(b)	Shear	74	NA	NA	NA	NA	NA	Shear	1.7
Shear	1.41	$60/A_0$	0.43	2(b)	Shear or microcrack	65	$522/S_0$	0.59	2(b)	Shear	85	Shear	2.8
Shear	1.097	$60/A_0$	0.43	2(b)	Shear or microcrack	65	$522/S_0$	0.6	2(b)	Shear	85	Shear	4.8
Shear	0.783	$60/A_0$	0.43	2(b)	Shear or microcrack	65	$270/A_0$	0.4	2(b)	Shear	28	Shear	8.2

Table A-2(c) Source identification process using ratios of WT peak magnitude ratio of 67.5˚/0˚ for microcrack initiation source

Source type	Depth (mm)	Primary freq. (kHz/mode)	Primary angle ratio	Table to consult	Conclusion from table	Percentage difference to next nearest source type	Secondary mode/freq. (kHz)	Secondary angle ratio	Table to consult	Conclusion from table	Percentage difference to next nearest source type	Final conclusion	Reduction factor = (Highest 0˚) /(lowest 45˚ peak)
Micro-crack	2.35	$522/S_0$	Zero differs from 67.5˚	2(b)	Not determined	NA	NA	NA	2(b)	NA	NA	Not determined	NA
Micro-crack	2.037	$60/A_0$	0.45	2(b)	Shear or microcrack	67	Zero differs from 67.5˚	NA	2(b)	Not determined	NA	Not determined	NA
Micro-crack	1.723	$60/A_0$	0.45	2(b)	Shear or microcrack	67	Zero differs from 67.5˚	NA	2(b)	Not determined	NA	Not determined	NA
Micro-crack	1.41	$60/A_0$	0.45	2(b)	Shear or microcrack	67	$270/A_0$	0.52	2(b)	Micro-crack	27	Micro-crack	6.5
Micro-crack	1.097	$60/A_0$	0.45	2(b)	Shear or microcrack	67	$270/A_0$	0.5	2(b)	Micro-crack	24	Micro-crack	6.2
Micro-crack	0.783	$60/A_0$	0.45	2(b)	Shear or microcrack	67	$270/A_0$	0.48	2(b)	Micro-crack	21	Micro-crack	5.9